

N Scaling of Large-Sample Collective Decay in Inhomogeneous Ensembles

Sergiy Stryzhenko,^{1,2} Alexander Bruns,¹ and Thorsten Peters¹

¹*Institut für Angewandte Physik, Technische Universität Darmstadt, Hochschulstraße 6, 64289 Darmstadt, Germany*

²*Institute of Physics, National Academy of Science of Ukraine, Nauky Avenue 46, Kyiv 03028, Ukraine*

(Dated: July 24, 2023)

Superradiance and -fluorescence are phenomena where N identical emitters coupled to each other synchronize and decay collectively N times faster than independent emitters would. This is accompanied by an intense burst whose peak photon rate is $\propto N^2$ for homogeneous excitation conditions. For inhomogeneous excitation, however, collective decay either cannot build up or its scaling breaks down, as different parts of the ensemble do not emit in sync. We here report on an experimental study of superfluorescence for a disordered ensemble of atoms coupled to a hollow-core fiber. The emitted radiation exhibits strong bursts, including a ringing. We demonstrate a decay rate enhanced by two orders of magnitude, despite intrinsic radial and longitudinal inhomogeneities. By devising a simple model, taking inhomogeneous broadening and light attenuation into account, we determine an effective number of collective emitters. We show that this recovers the N scaling known to homogeneous ensembles over a large range of parameters, as long as dispersion is negligible. Our results provide a simple physical understanding of the effects inhomogeneous conditions have on enhanced collective decay. This is relevant to optimize collective effects in extended ensembles as typically used in quantum optics, precision time-keeping or waveguide QED.

I. INTRODUCTION

The decay rate Γ at which an individual two-level system (TLS) emits radiation depends on its coupling to the available vacuum modes and can thus be altered when, e.g., placed inside a cavity [1]. If one considers an ensemble of N TLSs that are dipole-dipole coupled to each other via the emitted radiation, the decay can change significantly even without a cavity, as first noted by Dicke [2]. Due to the coupling, coherence can potentially build up between the emitters, leading to their spontaneous synchronization [3], and an enhanced collective decay rate $\Gamma_N > \Gamma$. This is termed superradiance (SR) [4, 5], if there is some initial coherence present, and superfluorescence (SF) [6] if the ensemble is initially completely inverted and coherence is initiated by vacuum fluctuations. Since its first observation [7], studies of enhanced collective decay were reported for various experimental platforms such as free-space [8–11] and waveguide-coupled atomic ensembles [12–15], quantum dots [16], superconducting qubits [17] and biological systems [18]. Besides being interesting due to its fundamental nature, applications of collective coupling can be found, e.g., in quantum optics [19], waveguide QED [20], astrophysics [21], atomic clocks [22, 23], and chemistry [18, 24].

There are several prominent features of collective decay [4]. Its increased decay rate is $\Gamma_N = \mu N \Gamma$, where μ and $\mu_N = \mu N$ are the single-atom and collective cooperativity [25], respectively. μ is a geometric factor describing the amount of spontaneously scattered radiation that can coherently couple to the ensemble of N emitters in the detected mode. Furthermore, a superradiant burst is emitted with a mean delay $\langle t_D \rangle$ after excitation, and its peak photon rate is $\propto N^2$. This burst occurs when $\langle t_D \rangle < \gamma^{-1}$, where γ is the decoherence rate of the TLSs. This determines a threshold condition to observe SR/SF.

Enhanced collective decay can be observed with small

samples, where the emitter density n is so high that multiple emitters are within a volume of the emitted wavelength λ , $n\lambda^3 \geq 1$ [26], as well as for large dilute samples, where $n\lambda^3 \ll 1$. In the latter case, propagation effects are important and excitation of the timed-Dicke state is crucial [27]. Here, the excitation is delocalized across the ensemble and a phase gradient is imprinted among *identical* emitters. Homogeneous excitation is thus of paramount importance. This can be challenging, especially for large samples. Therefore, it is not surprising that the effect of inhomogeneities on collective scattering are still actively investigated (see, e.g., [28–30]). Specifically in optically-dense ensembles, disorder [31], non-uniform phase shifts [32], off-resonant absorption [11, 33], finite switching times [34], as well as dispersion [35] were shown to affect the collective decay. In such conditions, several sub-systems can each radiate collectively only if the threshold condition is surpassed in each of them, while they all radiate independently from each other [29]. This leads to a breakdown of the textbook N scaling [11, 34, 36–38], potentially hiding the collective decay. As noted by Arecchi and Courtens [39], the number of cooperative emitters is effectively reduced when propagation losses, delays and inhomogeneous broadening become relevant. To account for this limited cooperation, they introduced the concept of maximum cooperation number (MCN) N_c , which replaces the total atom number N in the equations characterizing superradiant emission. Although determining a MCN for a given system would allow for understanding the physical limits to collective decay, this concept has so far, to the best of our knowledge, only been applied to cases where the length L of the ensemble is such that emitted radiation cannot interact with all atoms within the timescale of cooperation build-up [36, 37]. In optically-dense atomic ensembles [11, 31–33] or solid-state systems [38], where spectral and spatial inhomogeneities are relevant, how-

ever, this concept has never been applied.

In this paper we experimentally study large-sample SF for a broad range of inhomogeneous excitation conditions. With $N \leq 2.2 \times 10^5$ disordered atoms confined within a hollow-core photonic bandgap fiber (HCPBGF), we determine collective cooperativities $\mu_N \lesssim 300$. Due to intrinsic spatial and spectral inhomogeneities, the scaling of the experimental data can not be explained by textbook formulas considering the total number of atoms N . However, we will show that using a simple model to account for inhomogeneities allows for obtaining a MCN which recovers the textbook N scaling over a wide range of experimental parameters where dispersion is negligible. Our model allows for physical insight into the limits of collective decay in large ensembles, which is relevant to understand and optimize collective effects in, e.g., free-space [8–11, 40] or waveguide-coupled ensembles [13, 14, 20, 41–43]. In addition, our results are in agreement with the optical picture of linear-optics SR presented in [35, 44], showing the importance of attenuation and dispersion.

II. MODEL SYSTEM AND EXPERIMENTAL SETUP

We study SF for a disordered cold ensemble of ^{87}Rb atoms loaded into a single-mode HCPBGF [45, 46]. The waveguide provides long-range coupling between distant atoms, thereby facilitating the observation of collective effects [13, 47]. Employing a single-mode fiber avoids using a multi-mode theory to analyze the data [14]. The atoms are guided inside the fiber by a red-detuned Gaussian-shaped far-off-resonant trap (FORT), leading to an inhomogeneous radial atomic density profile of similar extension as the width of the near-Gaussian-shaped excitation field [see Fig. 1(c)] [46]. Moreover, as the ensemble can be made highly optically dense [45], attenuation of the excitation field has to be considered. Thus, the system exhibits large radial and longitudinal inhomogeneities. Due to an aspect ratio of the ensemble of order 10000 : 1, radiation trapping is expected to be negligible. In contrast to typical realizations of SR/SF where the excited state has a finite lifetime, we here study the decay of an effective TLS comprised of two long-lived ground states [see Fig. 1(a,b)] [48, 49]. An off-resonant excitation field (termed pump) scatters off an atomic ensemble prepared in $|1\rangle$. Once the pump is on, spontaneous Raman scattering induced by vacuum fluctuations initiates the decay, followed by a buildup of radiation bursts in the Stokes field. This was shown to be mathematically equivalent to superfluorescent decay in a true TLS [48]. The scattering rate of such an individual effective TLS is given by

$$\Gamma_R = R_B \Gamma \frac{\Omega_p^2}{4\Delta^2}, \quad (1)$$

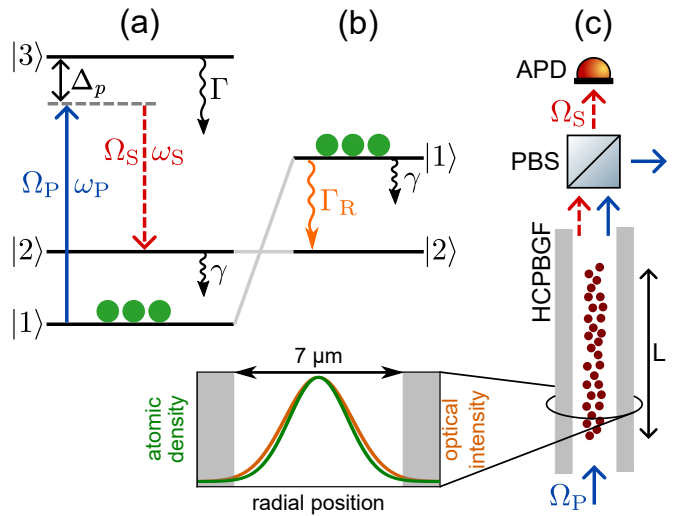


FIG. 1. (a) Simplified three level system with $|1\rangle \hat{=} ^2S_{1/2} F=1$, $|2\rangle \hat{=} ^2S_{1/2} F=2$, and $|3\rangle \hat{=} ^2P_{1/2} F'=2$. The excited state decay rate is $\Gamma = 2\pi \cdot 5.75 \text{ MHz}$ [50]. (b) Corresponding effective TLS comprised of the ground states $|1\rangle$, $|2\rangle$. (c) Simplified experimental setup.

where R_B is the branching ratio into the ground state $|2\rangle$, Γ is the excited state decay rate, and Ω_p is the Rabi frequency of the pump field effectively detuned from the transition $|1\rangle \leftrightarrow |3\rangle$ by $\Delta = \Delta_p + 2S$. Here, Δ_p is the externally applied detuning and $2S = 2\Omega_p^2/(4\Delta_p)$ is the AC Stark shift of the transition frequency due to the strong and detuned pump field.

Using such effective TLS to study SR/SF has several advantages over real TLSs. First, the decay rate Γ_R is not fixed and can be tuned by the intensity and detuning Δ_p of the pump field. Second, Γ_R can be made much smaller than the excited state decay rate Γ , which sets the width of the dispersive resonance. Thus, even for large decay rates $\Gamma_N \gg \Gamma_R$ we still can have $\Gamma_N < \Gamma$, and dispersive effects as discussed in [35] are more likely to be negligible. This leads to a significant simplification when modeling the MCN. Third, the modulation bandwidth of the excitation field has to be larger than Γ_N . This can be technically challenging if the single-atom decay rate Γ is already quite large [34], but is no issue in the case presented here.

Figure 1(c) shows our simplified experimental setup. A detailed description including the procedure to load atoms into the HCPBGF (NKT Photonics, HC-800-02) can be found in [46]. Therefore, we only give a brief summary here. First, we load a magneto-optical trap with around 10^7 ^{87}Rb atoms. Then, we shift the cold atom cloud towards the HCPBGF tip while compressing it radially using magnetic fields. Here, up to 2.5% of the atoms are loaded into the FORT emerging from the HCPBGF with a numerical aperture of $\text{NA} \sim 0.092$. The FORT guides the atoms radially inside the fiber, while they are basically free-falling in the longitudinal (verti-

cal) direction. The atomic ensemble exhibits a Gaussian radial distribution of $1/e$ half width $\sigma_a \sim 1.7 \mu\text{m}$ and a length of $L \sim 3 \text{ cm}$. Inside the HCPBGF we prepare the atoms in state $|1\rangle$ by optical pumping without specific preparation of Zeeman levels. Subsequently, the linear-polarized pump beam is launched into the fiber in such a way that its polarization is maintained at the exit to allow for efficient polarization filtering [51]. Its temporal intensity is controlled by an acousto-optic modulator with a rise time of $\tau_p = 130(5) \text{ ns}$. The radial intensity has a near-Gaussian profile with a $1/e^2$ half-width of $\sigma_p \sim 2.75 \mu\text{m}$. We detect the transmitted light using an avalanche photodiode (APD, Laser Components SAR500H1B) and a digital oscilloscope.

III. EXPERIMENTAL STUDIES

In the following we study SF decay in the effective TLS shown in Fig. 1. Before each measurement, we switch off the trapping potential to avoid inhomogeneous broadening by the FORT. When the pump is resonant with $|1\rangle \leftrightarrow |3\rangle$ we can measure N by time-resolved optical pumping [46]. The measured shot-to-shot fluctuations of N are $\lesssim 3.5\%$. We then detune the pump field from the transition $|1\rangle \leftrightarrow |3\rangle$ by a variable amount Δ_p . We observe the temporally-resolved Stokes radiation by detecting light orthogonally polarized to the pump. As confirmed by measurements and a numerical simulation, the polarization of the Stokes field is predominantly linear and orthogonal to the pump field. This allows for efficient discrimination between the two fields using a polarizing beam splitter (PBS). We show in Fig. 2(a) exemplary data for the transmitted pump power through the HCPBGF without atoms (blue) and for the transmitted Stokes power P_s with $N = 83 \times 10^3$ atoms loaded into the HCPBGF (orange) versus time, where $t = 0$ corresponds to the moment the pump power reaches 50% of its mean maximum value. After the pump has been switched on there is a fluctuating delay of several hundred nanoseconds during which no Stokes light is detected. Then, however, a fast burst is suddenly emitted with a fluctuating peak power P_s (i.e., photon rate), followed sometimes by another burst of smaller peak power due to a coherent ringing [4, 52]. This trace, showing a large first burst followed sometimes by a smaller one, represents the dominant temporal shape of the emitted Stokes light for $N < 220 \times 10^3$. For our maximum attainable $N = 220 \times 10^3$, however, the shape changes, as shown in Fig. 2(a) by the green trace. Here, a more pronounced ringing is observed and the second burst is becoming dominant. In order to obtain good statistics for the observed Stokes emission, we repeat the measurement for each set of experimental parameters (N, Δ_p) 100 times (video). As we can see from the huge shot-to-shot fluctuations in amplitude, delay, intensity and shape, the Stokes signal shows the typical signature of SF bursts due to its initiation by vacuum fluctuations [53, 54]. The

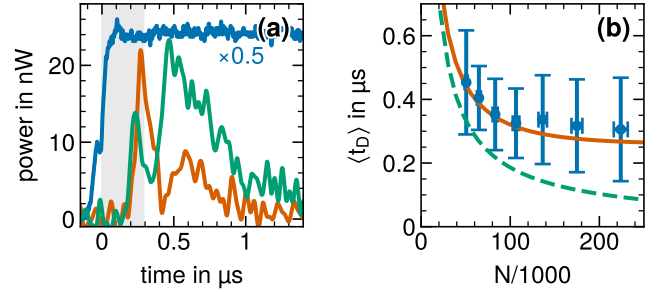


FIG. 2. (a) Exemplary single-shot traces of the transmitted pump power without atoms (blue, scaled down by factor of 0.5) and the Stokes power with atoms loaded into the HCPBGF. The peak Rabi frequency is $\Omega_p^{(0)} = 6.4\Gamma$, $\Delta_p = 18.4\Gamma$ with $N = 83 \times 10^3$ (orange) and $N = 220 \times 10^3$ (green). The extracted delay (grey shaded area) is $t_D = 290 \text{ ns}$. (b) Measured mean delays of the first emitted SF burst vs. total atom number N for $\Delta_p = 18.4\Gamma$. The error bars represent the standard deviation of the data. The expected theoretical dependence [Eq. (2)] is shown considering the total atom number N (dashed green line) as well as the MCN N_c (orange solid line) for $\beta = 0.07$.

Stokes burst dynamics occur on a timescale much shorter than expected for the calculated single-atom scattering rate of $\langle \Gamma_R \rangle_r = 2\pi \times 45 \text{ kHz}$, where $\langle \dots \rangle_r$ denotes a radial average over the Gaussian-shaped pump intensity and atomic density distributions (see App. B). From each single dataset we extract the delay and peak power of the first emitted Stokes burst by an automated algorithm to finally obtain the mean delay $\langle t_D \rangle$ and mean peak power $\langle P_s \rangle$, including their respective standard deviations.

Fig. 2(b) shows exemplary data for the measured mean delays vs. the total atom number N (symbols). Ω_p and Δ_p are the same as in Fig. 2(a) and we expect the system to be well-described by an effective TLS. The standard deviations from the mean delay are significant $\sim 38\%$, which is again a signature of vacuum fluctuations initiating the decay process [53, 54]. In the same plot we show the expected dependence (blue solid line) for a homogeneous system [55]

$$\langle t_D(N) \rangle = \frac{1}{4\mu N \Gamma_R} \left[\ln \sqrt{2\pi N} \right]^2. \quad (2)$$

The measured data exhibit larger delays than expected from theory, which is typical for inhomogeneously-broadened systems [56].

As to determine the collective decay rate Γ_N from our data showing non-exponential decay with strong bursts, we calculate $\Gamma_N = \left[\ln \sqrt{2\pi N} \right]^2 / (4\langle t_D \rangle)$ using the measured mean delay and total atom number. In Fig. 3(a) we show the results for the collective cooperativity $\mu_N^{(\text{exp})} = \Gamma_N / \langle \Gamma_R \rangle_r$ vs. the total atom number N for a large range of detunings, along with the expected theoretical dependence $\mu_N = \mu N$ (blue line). Here, we set $\mu \approx N \text{A}^2 / 4 = 2.1 \times 10^{-3}$. The collective cooperativ-

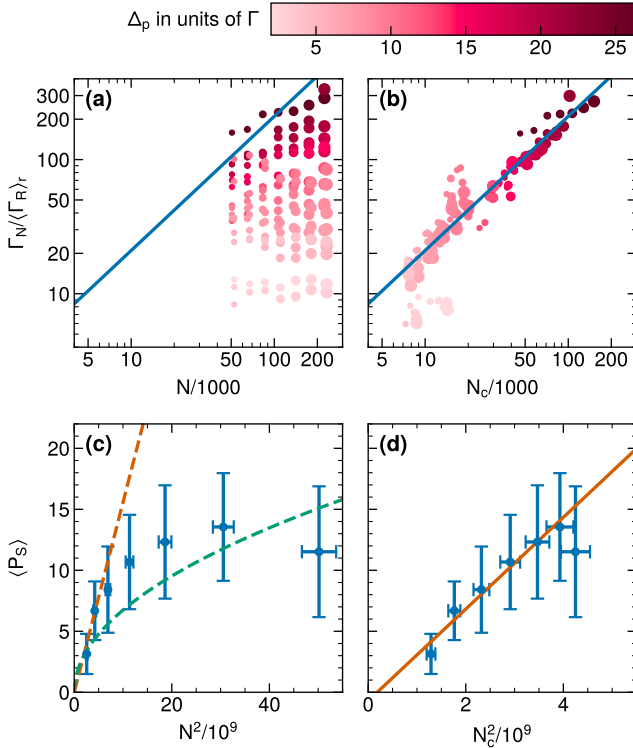


FIG. 3. (a,b) Collective cooperativity vs. total atom number N (a) and MCN N_c (b). We determined the collective cooperativity from the measured mean delays (see text) for detunings $2\Gamma \leq \Delta_p \leq 26.4\Gamma$ at $\Omega_p^{(0)} = 6.4\Gamma$. The symbol size is proportional to N . The solid blue lines show the expected dependence μ_N, μ_{N_c} for homogeneous SR theory. (c,d) Measured mean peak power of the first emitted SF burst vs. N^2 (c) and N_c^2 (d) for $\Delta_p = 18.4\Gamma$. The green (orange) dashed line in (c) represents a linear (quadratic) scaling with N for reference. The orange solid line in (d) represents a least-squares linear fit to the data, excluding the last data point (see text).

ity $\mu_N^{(\text{exp})}$ is significantly enhanced by more than two orders of magnitude. It scales approximately linearly with N but only at the largest detunings for each of which the slope is different. Moreover, the experimental data does not collapse onto $\mu_N = \mu N$ (blue line) expected for homogeneous conditions, except for the lowest N and largest Δ_p . Close to resonance, $\mu_N^{(\text{exp})}$ is approximately independent of N . Thus, N is not a good scaling parameter. We next determine the dependence of the peak Stokes power on N . To this end we plot in Fig. 3(c) the measured $\langle P_S(N^2) \rangle$ (symbols). We observe a N^2 scaling (dashed orange line) only for small N . As N becomes larger, the scaling approaches a linear dependence (dashed green line) as expected for independent emitters. This change in scaling indicates a significant reduction in cooperativity for increasing N . A similar behavior is seen for other detunings with a breakdown of N^2 scaling occurring for smaller N as Δ_p becomes smaller.

Our results clearly demonstrate strong collective decay for our disordered atomic ensemble coupled to an HCP-BGF. However, the in part significant deviations from theory for homogeneous conditions evoke a deeper investigation as to understand the limits to collective emission in our system and to optimize it. To this end, we determine in the following the fraction of atoms $N_c = \eta N$ which can radiate collectively, i.e., can be viewed as homogeneously driven. This approach is based on the concept of MCN [39]. We identify two major mechanisms which affect the MCN. (i) Inhomogeneous broadening, and (ii) pump attenuation. In the following we will address each of them individually. Although pump attenuation leads to an inhomogeneity as well, we make a distinction as will become clear later. Note that due to the radial as well as longitudinal dependence of the pump intensity determining decay rate, AC Stark shift, and Stokes gain, we factorize the problem to allow for obtaining some simple analytical expressions. We thus first determine radially-averaged quantities and then apply them to average longitudinally. See App. B for additional details on the following model.

First, we consider *inhomogeneous broadening*. As noted in [39], the number of cooperative scatterers is reduced by the ratio $\sigma_{\text{hom}}/\sigma_{\text{inh}}$ of (homogeneous) excitation bandwidth and inhomogeneous linewidth if $\sigma_{\text{hom}} < \sigma_{\text{inh}}$. The excitation bandwidth is given by $\sigma_{\text{hom}} \sim 1/\tau_p$. We estimate the inhomogeneous linewidth $\sigma_{\text{inh}} = \delta S + \delta\Gamma_R$ as being determined by the standard deviations of the ground state AC Stark shift δS and the scattering rate $\delta\Gamma_R$ from their radial averages $\langle S(r) \rangle_r = \langle \Omega_p^2(r) \rangle_r / (4\Delta_p)$ and $\langle \Gamma_R(r) \rangle_r$, respectively (see Eq. (B5) in the Appendix). This yields a first correction factor $\eta_{\text{inh}} = 1/(\tau_p \sigma_{\text{inh}})$ to the MCN. Next, we consider *pump attenuation* along the propagation direction z through the optically-dense ensemble. Such attenuation was shown to be detrimental to the excitation of the timed-Dicke state [32, 33], and in our case directly affects the decay rate of the effective TLS. We thus first take (off-)resonant absorption $I_p(\Delta_p, z') = I_p^{(0)} \exp[-\alpha(\Delta_p)z']$ with $z' = z/L$ according to the Beer-Lambert law into account. Here we approximate $\alpha(\Delta_p) \approx \langle \alpha(\Delta_p, 0) \rangle_r = \langle \alpha_0 \Gamma^2 / \{4[\Delta_p + 2S(r, 0)]^2\} \rangle_r$ by its initial value at $z' = 0$, where α_0 is the resonant optical depth, and we performed an radial average. Noting further that the Stokes intensity eventually grows as $I_s \sim \exp[G_s(\Delta_p)z']$ [48, 55], where the Stokes gain $G_s(\Delta_p, 0) \approx \langle 2\alpha_0 \Gamma_R(\Delta_p, 0) / \gamma \rangle_r$, we next consider pump attenuation due to conversion into the Stokes field. Here, γ is the ground state decoherence rate and $G_s > 1$ for all our experimental parameters. We thus make the ansatz $I_p(z') \approx I_p^{(0)} \exp[-\tilde{\alpha}(\Delta_p)z']$ for the pump intensity, where the total attenuation factor is $\tilde{\alpha}(\Delta_p) = \alpha(\Delta_p, 0) + \beta(\Delta_p)G_s(\Delta_p, 0)$. In a first approximation we assumed that $\tilde{\alpha}(\Delta_p)$ is given by its initial radially-averaged value at $z' = 0$. As this ansatz corresponds to considering only steady-state instead of also

transient conditions during Stokes field buildup, the latter of which exhibit a time-dependent Stokes intensity evolution [48], we introduced a scaling factor $\beta(\Delta_p)$ for the Stokes gain as the only free parameter in our model. We next calculate the effective collective decay rate as

$$\langle \Gamma_N^{\text{eff}} \rangle_{r,z} = \mu N \cdot \frac{2}{\sigma_a^2} \int_0^1 dz' \int_0^\infty dr r e^{-\frac{r^2}{\sigma_a^2}} \Gamma \times \frac{\Omega_p^2(r, z')}{8 [\Delta_p + 2S(r, z')]^2}, \quad (3)$$

where $\Omega_p(r, z') = \Omega_p^{(0)} \exp(-r^2/\sigma_p^2) \exp[-\tilde{\alpha}(\Delta_p)z'/2]$ and we used $R_B = 0.5$ according to our coupling scheme. Following [57, 58] we can now determine a shadow factor $\eta_s = \langle \Gamma_N^{\text{eff}} \rangle_{r,z} / \langle \Gamma_R \rangle_r$ taking attenuation of the excitation field into account. Here, $\langle \Gamma_R \rangle_r$ is the radially-averaged single-atom scattering rate at $z' = 0$ used as a reference without attenuation. Combining inhomogeneous broadening and pump attenuation, we finally determine the MCN as

$$N_c = \eta_{\text{inh}} \cdot \eta_s \cdot N. \quad (4)$$

To test our simple model, we calculate $\langle t_D(N_c) \rangle$ using N_c instead of N in Eq. (2) by manually adjusting β as the only free parameter to yield the best agreement with the experimental data. Exemplary results are shown in Fig. 2(b) by the orange solid line for $\beta = 0.07$, which agrees much better with the experimental data than the dashed green line using N . Employing a constant β to calculate the mean delays works satisfactory for $\Delta_p > 7\Gamma$ to reproduce our experimental data for all N . However, allowing for a varying $\beta = \beta(\Delta_p)$ (probably incorporating a complicated to calculate spatio-temporal evolution of the Stokes gain) improves the agreement even further. The resulting $\beta(\Delta_p)$ is shown in Fig. 6 of the appendix. In the range of detunings $\Delta_p \gtrsim \Omega_p$ where our effective TLS model should be valid, β scales approximately linearly with Δ_p . The origin of this dependence is currently unknown. For smaller Δ_p , β increases dramatically, indicating that our model can not be applied in this range. We therefore use $\beta(\Delta_p) = 0.182 - 6.1 \times 10^{-3} \Delta_p / \Gamma$ as determined by a linear fit for $\Delta_p > 6\Gamma$ to calculate $N_c(\Delta_p, N)$ for all our data. The results for the relative MCN $N_c(\Delta_p, N)/N$ are shown in Fig. 4. As we can see, only for the smallest N and largest Δ_p the MCN is close to N . As N increases and Δ_p decreases, however, the MCN reduces to $N_c \sim 0.1N$, i.e., only 10% of the total number of atoms contribute to collective scattering for these parameters. Using these calculated MCNs, we can now plot the collective cooperativity $\mu_N^{(\text{exp})}(N_c)$ and the mean peak Stokes power $\langle P_s(N_c^2) \rangle$, respectively. The results are shown in Fig. 3(b,d). In contrast to Fig. 3(a) where the total atom number N was used, $\mu_N^{(\text{exp})}$ collapses onto the linear dependence μN_c over a large range of detunings and atom numbers where our effective TLS model should be valid. Moreover, we also observe a

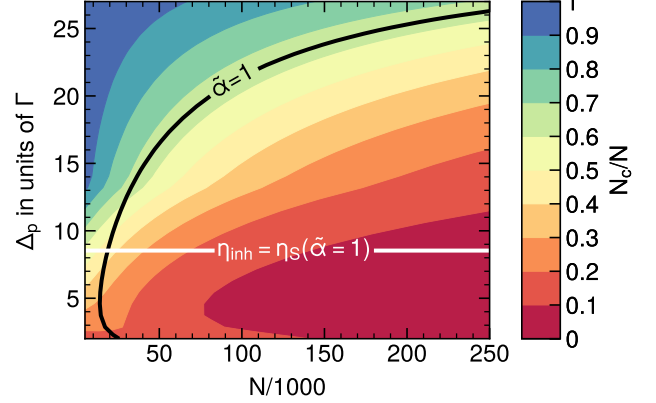


FIG. 4. Relative MCN $N_c(\Delta_p, N)/N$ vs. total atom number N and detuning Δ_p for our experimental parameters. The black line shows where the total attenuation factor $\tilde{\alpha} = 1$. The white line indicates where the inhomogeneous scaling factor $\eta_{\text{inh}} = \eta_s(\tilde{\alpha}=1)$.

quadratic scaling of $\langle P_s \rangle$ with the MCN over almost the full range of atom numbers N where the first SF burst is dominant. Only at the largest N the scaling of $\langle P_s \rangle$ changes. Here, however, the dominant temporal shape of Stokes bursts changes as shown by the green trace in Fig. 2(a). Now the second instead of the first burst exhibits the largest power, which is not the case in standard SR theory [4]. Therefore, it is not surprising that the scaling changes and we thus exclude this data point in the fitting procedure.

These results demonstrate that the concept of MCN can recover the homogeneous scaling of collective decay for inhomogeneous conditions. The obvious question arising is for which parameters are inhomogeneous broadening and/or pump attenuation limiting the MCN in our setup? We therefore plot in Fig. 4 the boundary for which the calculated $\tilde{\alpha}(\Delta_p, N) = 1$ (black line). Here, the pump intensity drops to $1/e$ of its initial value which was shown having a detrimental effect on collective decay [11, 33]. Similarly, we plot the boundary for which $\eta_{\text{inh}} = \eta_s(\tilde{\alpha}=1)$ (white line). As we can see, our system is limited by pump attenuation for large detunings where inhomogeneous broadening is still negligible. Only for detunings $\Delta_p \lesssim 9\Gamma$ inhomogeneous broadening is becoming relevant. This demonstrates that a parameter regime can be found for atomic ensembles coupled to hollow-core fibers, for which the intrinsic radial inhomogeneities can be rendered insignificant. Moreover, by choosing an appropriately large detuning, almost all atoms can contribute to collective scattering, leading to a pronounced enhancement of the collective decay rate, at least as long as dispersion is negligible.

IV. DISCUSSION AND OUTLOOK

Despite the significant simplifications made, our model seems to capture the relevant physics. Only for detunings $\Delta_p \lesssim 7\Gamma$ deviations from the experimental data become more significant. This range is however similar to the range where the approximation of an effective TLS is not valid anymore for $\Omega_p^{(0)} = 6.4\Gamma$. A corresponding increase of β is therefore not surprising. Simultaneously, dispersion is likely to become relevant [35] as $(\Delta_p - \Gamma_N) / \sqrt{\Gamma^2 + 2\Omega_p^2} \lesssim 1$, i.e., frequency components of the SF bursts are lying within the dispersive bandwidth of the excited state. This is currently not captured by our model. It would be interesting trying to determine a further scaling factor in addition to η_{inh} and η_s which contains the effect of dispersion on the MCN. As dispersion becomes relevant in our system only when the effective TLS model is no more valid, true TLSs, e.g., as in [11], ought be better suited for such investigations. This would also allow for neglecting attenuation of the excitation field due to conversion, which contains the only free parameter in our model. Such study could lead to finding an analytical model for dispersive ensembles which explains experimental results [59]. Intuitively we would expect that combining inhomogeneous broadening, attenuation and dispersion leads to the simple picture that enhanced collective decay disappears as soon as the MCN becomes $N_c = 1/\mu$. The other interesting regime that might be worth studying is that of large N where the temporal shape of SF bursts exhibiting a smaller first burst followed by a larger second one becomes dominant [see green trace in Fig. 2(a)]. This is in contrast to typical SF burst shapes [4, 34, 52]. Although we could find similar shapes in the literature on stimulated Raman scattering [60], they were reported as more unlikely compared to the shape with decreasing burst amplitudes.

Besides supporting a rather simple physical picture of enhanced collective decay (with negligible dispersion), our results could be relevant to large-sample systems such as in astrophysics [21], waveguide-coupled ensembles [20], atomic clocks [22, 23], and quantum optics [19]. Specifically in the latter field collective scattering plays an important role in the read-out of stored quanta [8]. Moreover, SF could also be used during the pair-generation process in quantum light sources based on spontaneous four-wave mixing [61] leading to low-power non-classical photon sources.

V. SUMMARY

In summary we presented an experimental study of superfluorescence in a disordered ensemble of cold atoms coupled to a hollow-core fiber. We demonstrated a decay rate collectively-enhanced by more than two orders of magnitude for $N \lesssim 2.2 \times 10^5$ atoms. By implementing an effective TLS we were able to study the decay with negli-

gible dispersion for a large range of detunings and optical depths. Thereby we could tune the amount of inhomogeneity, studying its effect on the SF decay and developing a simple theoretical model considering inhomogeneous broadening and attenuation of the excitation field. Using this model, we determined a maximum cooperation number N_c of atoms that can be treated homogeneously and thus decay collectively. Depending on the detuning and atom number, N_c varied between 10%–90% of the total atom number. We demonstrated that using N_c instead of N , the N scaling known to collective decay in homogeneous ensembles could be recovered. This allowed for a physical understanding of the limits to enhanced collective decay in our waveguide-coupled ensemble. Our results provide a simple tool to optimize enhanced collective scattering in inhomogeneous extended ensembles, potentially also such exhibiting significant dispersion.

ACKNOWLEDGMENTS

The authors would like to thank W. Guerin and L.P. Yatsenko for discussions, E. Giese, R. Walser, and V. Stojanovic for discussions and comments on the manuscript, and T. Halfmann for his continuous support and comments on the manuscript. We acknowledge the group of T. Walther for providing us with their home-built ultra-low noise laser diode driver with high modulation bandwidth. The project received funding from the European Union's Horizon 2020 research and innovation programme under the Marie Skłodowska-Curie grant agreement No. 765075 and by the Deutsche Forschungsgemeinschaft (DFG, German Research Foundation) project number 410249930.

Appendix A: Determination of Experimental Parameters For the Theoretical Model

Comparing the experimental data to the theoretical model requires knowledge of several experimental parameters. The geometric factor describing the fraction of spontaneous light emitted into the fiber core mode is approximately given by $\mu \approx \text{NA}^2/4$, where NA is the numerical aperture of the HCPBGF. Taking the measured $1/e^2$ mode field radius $\sigma_p = 2.75 \mu\text{m}$ of the near-Gaussian-shaped intensity distribution, we determine $\text{NA} = \lambda/(\pi\sigma_p) = 0.092$ with $\lambda = 795 \text{ nm}$. This results in $\mu = 2.1 \times 10^{-3}$. The decay rate of the effective TLS depends on the Rabi frequency Ω_p of the pump and its detuning Δ_p , as does the AC Stark shift S . We measure the pump power at a certain location inside the experimental setup and correct for transmission losses from the HCPBGF to this location. Then, using the measured mode field diameter, we calculate the peak Rabi frequency $\Omega_p^{(0)}$ according to the parameters given in [50]. The detuning Δ_p is controlled by the frequency of the acousto-optic modulator (AOM) modulating the

pump with a rise time $\tau_p = 130(5)$ ns. The frequency uncertainty of the AOM is negligible leaving only the uncertainty of the pump laser lock-point. We estimate this uncertainty as $\lesssim \Gamma/10$, which can therefore be neglected as well in our analysis. The total atom number N is determined as described in the main article with a shot-to-shot uncertainty of 3.5 %. The radial atomic density profile was investigated in [46] from which we assume a Gaussian-shaped radial density with a $1/e$ half width of $\sigma_a = 1.7 \mu\text{m}$. Using an atomic density, $n(r, z) = n(r)$, and $\Omega_p(r)$, we determine the peak optical depth as

$$\alpha_0 = \frac{4}{\sigma_p^2} L \int_0^{r_c} dr r \sigma_{13} n(r) e^{-\frac{2r^2}{\sigma_p^2}}, \quad (\text{A1})$$

where σ_{13} is the resonant absorption cross-section of the $|1\rangle \leftrightarrow |3\rangle$ according to [50], r_c is the core radius of the HCPBGF and we determined $n(r)$ such that $2\pi L \int dr r n(r) = N$. As the final parameter to determine, there is a residual decoherence rate between the two ground states due to residual magnetic field gradients and time-of-flight broadening once the guiding potential is off for the measurements. This value was determined from light storage and retrieval experiments as $\gamma_0 \sim 0.057(6)\Gamma$ [61].

Appendix B: Determination of the Maximum Cooperation Number

In the following we present the model used to calculate the maximum cooperation number N_c . It is mainly based on the ideas presented by Arecchi and Courtens [39], Binenaimé *et al.* [33], and Bachelard *et al.* [57]. First, inhomogeneous broadening reduces the number of cooperative atoms [39]. Second, attenuation of the pump field as it propagates through the optically-dense ensemble reduces the effective scattering/decay rate, i.e., number of scatterers. We account for this by calculating a factor η_s from an effective scattering rate in the spirit of the shadow effect introduced by Bachelard *et al.* [57]. We note that in our case the decay rate Γ_R itself depends on the (attenuated) excitation field, which is in contrast to decay in a true TLS where the decay rate is constant and only the excitation is inhomogeneous.

To find a simple analytical model, we make several assumptions, as the actual system exhibits complicated nonlinear spatial and temporal dynamics. First, there is a radial variation of the atomic density distribution $n(r) = n_0 \exp(-r^2/\sigma_a^2)$, and we assume a constant density along the propagation direction z . Second, the pump intensity $I_p(r, z) \propto \Omega_p^2(r, z)$, determining both Raman scattering rate and AC Stark shift of the ground state, is potentially attenuated along the propagation direction z and also exhibits a radial variation $\Omega_p^2(r, 0) = \Omega_p^2(0, 0) \exp(-2r^2/\sigma_p^2)$. Its $1/e^2$ half width is only slightly larger than σ_a . In order to find a simple analytical model, we use the fact that $\Omega_p^2(r, z)$ can be factorized

as

$$\Omega_p^2(r, z) = \Omega_p^2(0, 0) \cdot f_p(r) \cdot g_p(z), \quad (\text{B1})$$

Furthermore, inhomogeneous broadening due to the radial variations is expected to dominate over longitudinal variations as it is also present for large detunings. These assumptions allow for considering the radial and longitudinal variations independently. In the following we start by calculating the radial averages weighed by the atomic density distribution at the start of the medium at $z = 0$ for obtaining the inhomogeneous linewidth. Then, we take the radial and longitudinal average to determine the effective scattering rate. Using these results we then determine a MCN.

1. Inhomogeneous Broadening

As discussed by Arecchi and Courtens, inhomogeneous broadening reduces the number of cooperative atoms by the ratio of (homogeneous) excitation bandwidth σ_{hom} to inhomogeneous linewidth σ_{inh} [39]. The excitation bandwidth can be estimated by the rise time τ_p of the pump field, $\sigma_{\text{hom}} = 1/\tau_p$. The inhomogeneous linewidth of the effective TLS can be estimated as follows. The pump intensity inside the HCPBGF determines the AC Stark shift S of the ground state $F=1$

$$S(r, z) = \frac{\Omega_p^2(r, z)}{4\Delta_p} \quad (\text{B2})$$

and the Raman scattering rate of the effective TLS

$$\Gamma_R(r, z) = \Gamma \frac{\Omega_p^2(r, z)}{8 [\Delta_p + 2S(r, z)]^2}. \quad (\text{B3})$$

We therefore calculate the radial averages of $\Omega_p^2(r, 0)$, $S(r, 0)$, and $\Gamma_R(r, 0)$ at the beginning of the medium at $z = 0$ weighed by the atomic density distribution as

$$\langle f(r) \rangle_r = \frac{2}{\sigma_a^2} \int_0^\infty dr r e^{-\frac{r^2}{\sigma_a^2}} f(r), \quad (\text{B4})$$

where $f(r) = [\Omega_p^2(r, 0), S(r, 0), \Gamma_R(r, 0)]$.

Using the radially-averaged values, we now estimate the inhomogeneous linewidth σ_{inh} as follows. Due to the radial Gaussian dependence of the pump field, atoms in the ensemble of radial width σ_a will experience an inhomogeneous AC Stark shift $S(r)$ of the ground state $F=1$ due to the strong pump beam as well as an inhomogeneous decay rate $\Gamma_R(r)$. As a measure for the corresponding linewidth we calculate the standard deviation

$$\delta f = \sqrt{\langle [f(r) - \langle f(r) \rangle_r]^2 \rangle_r} \quad (\text{B5})$$

for $f(r) = [S(r, 0), \Gamma_R(r, 0)]$ and set

$$\sigma_{\text{inh}} = \delta S + \delta \Gamma_R. \quad (\text{B6})$$

Using the measured rise time τ_p of the pump pulse, we obtain the first of two scaling factors,

$$\eta_{\text{inh}} = \frac{1}{\tau_p \sigma_{\text{inh}}}, \quad (\text{B7})$$

to calculate the MCN. Note that we only apply this scaling factor if the inhomogeneous bandwidth is larger than the homogeneous bandwidth.

2. Effective Scattering Rate

Having determined a scaling factor which accounts for inhomogeneous broadening (in the radial direction), we next turn to the variations in the longitudinal direction z . This is relevant for our considered system, as propagation through the optically-dense atomic ensemble can attenuate the pump field. To this end, we calculate an effective collective scattering rate weighed by the radial atomic density distribution $n(r)$

$$\langle \Gamma_N^{\text{eff}} \rangle_{r,z} = \mu N \cdot \frac{2}{\sigma_a^2} \int_0^1 dz' \int_0^\infty dr r e^{-\frac{r^2}{\sigma_a^2}} \Gamma \times \frac{\Omega_p^2(r, z')}{8 [\Delta_p + 2S(r, z')]^2}, \quad (\text{B8})$$

where

$$\Omega_p(r, z') = \Omega_p^{(0)} e^{-\frac{r^2}{\sigma_p^2}} e^{-\frac{1}{2} \tilde{\alpha}(\Delta_p) z'}, \quad (\text{B9})$$

and $\Omega_p^{(0)} [= \Omega_p(0, 0)]$ is the peak Rabi frequency of the pump. We assume attenuation of the pump intensity according to Beer-Lambert's law along the dimensionless distance $z' = z/L$ with an attenuation factor $\tilde{\alpha}(\Delta_p)$ affecting also $S(r, z')$ in Eq. (B2). We obtain the corresponding collective scattering rate $\langle \Gamma_N \rangle_r$ without pump attenuation by setting $\tilde{\alpha}(\Delta_p) \equiv 0$ in Eq. (B8). Similar to Bachelard *et al.*, where a *shadow factor* was defined to determine an effective reduction in the total scattering cross-section of an optically-dense ensemble [57], we now define a shadow factor

$$\eta_s = \frac{\langle \Gamma_N^{\text{eff}} \rangle_{r,z}}{\langle \Gamma_R \rangle_r}, \quad (\text{B10})$$

where $\langle \Gamma_R \rangle_r$ is the radially-averaged single-atom scattering rate at $z' = 0$ used as reference without attenuation. η_s is thus a measure for the reduction of the collective scattering rate due to pump attenuation. As $\langle \Gamma_N^{\text{eff}} \rangle_{r,z} \propto N$ we identify $\eta_s N$ as an effective number of atoms that will scatter collectively when considering attenuation of the pump field.

3. Maximum Cooperation Number

Finally, combining inhomogeneous broadening and longitudinal pump attenuation, we determine the MCN

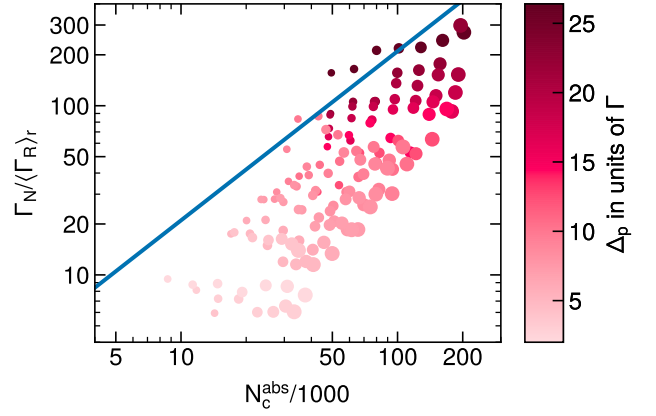


FIG. 5. Collective cooperativity $\Gamma_N/\langle \Gamma_R \rangle_r$ vs. N_c^{abs} when considering inhomogeneous broadening and pump attenuation due to off-resonant absorption. The symbol size is proportional to N . The solid line shows the dependence μN_c^{abs} .

as

$$N_c = \eta_{\text{inh}} \cdot \eta_s \cdot N. \quad (\text{B11})$$

Appendix C: Modeling Pump Attenuation

In order to apply the general model described above to our experimental data, we need to identify which factors cause attenuation of the pump, i.e., we need to model the (dimensionless) attenuation factor $\tilde{\alpha}(\Delta_p)$. The first obvious consideration is (off-)resonant absorption. Our experiment allows for loading $N \lesssim 2.2 \times 10^5$ atoms into the HCF. With an OD per atom of $\alpha^* = 2.75 \times 10^{-3}$ on the transition $^2S_{1/2} F=1 \leftrightarrow ^2P_{1/2} F'=2$ we therefore achieve resonant optical depths of $\alpha_0 \lesssim 600$. The detuning-dependent optical depth at $z = 0$ for large detunings is approximately given by

$$\alpha(\Delta_p) \approx \alpha_0 \left\langle \frac{\Gamma^2}{4 [\Delta_p + 2S(r, 0)]^2} \right\rangle_r, \quad (\text{C1})$$

where we have taken a radial average (see App. B 1). For our experimental parameters we reach $\alpha(\Delta_p) \gtrsim 1$ for $\Delta_p \lesssim 12\Gamma$. Setting $\tilde{\alpha}(\Delta_p) \equiv \alpha(\Delta_p)$ in Eq. (3), where we assumed in a first approximation that the attenuation factor does not depend on z and is given by its initial value at $z = 0$, yields a MCN N_c^{abs} for each data point in Fig. 3(a). Plotting the collective cooperativity vs. N_c^{abs} we obtain the plot shown in Fig. 5. Note that there is no free fitting parameter. Obviously, N_c^{abs} is a better scaling parameter than the total atom number N . Yet the data points do not collapse onto the blue line showing μN_c^{abs} .

We therefore consider additional attenuation of the pump. To this end we note that the Stokes buildup happens on a timescale determined by the Stokes gain [48] and that the derivation of Eq. (2) was done in a regime of

exponential growth of the SF burst [55]. We thus make the ansatz

$$I_p(z') \approx I_p^{(0)} e^{-\tilde{\alpha}(\Delta_p)z'}, \quad (\text{C2})$$

where the total attenuation factor is given by

$$\tilde{\alpha}(\Delta_p) = \alpha(\Delta_p) + \beta(\Delta_p) \cdot G_s(\Delta_p, 0). \quad (\text{C3})$$

We thus assume that the pump intensity I_p decreases exponentially due to absorption *and* conversion into the exponentially-growing Stokes field $I_s(z') \propto \exp(\beta(\Delta_p)G_s(\Delta_p, 0)z')$ with a scaling factor $\beta(\Delta_p)$.

The initial radially-averaged Stokes gain can be approximately written as

$$G_s(\Delta_p, z'=0) \approx \alpha_0 \left\langle \frac{2\Gamma_R(\Delta_p, 0)}{\gamma} \right\rangle_r, \quad (\text{C4})$$

where γ is the ground state decoherence rate. For our all our experimental parameters we determine $G_s(\Delta_p, z'=0) > 1$. This ansatz corresponds to steady-state conditions in [48] while neglecting transient conditions during Stokes field buildup, as during the latter one the Stokes intensity evolution is additionally time-dependent which complicates the theoretical description [48]. To account for this simplification we introduced the scaling factor $\beta(\Delta_p)$, which is allowed to vary with Δ_p (see App. D).

In order to calculate the initial Stokes gain, we have to determine the decoherence rate γ . We identify three major contributions to γ for our effective TLS. First, there is a residual decoherence rate between the two ground states determined by residual magnetic field gradients and time-of-flight broadening. This value was determined from light storage and retrieval experiments as $\gamma_0 \sim 0.057(6)\Gamma$ [61]. Second, the inhomogeneous AC Stark shift of the the ground state by the pump field causes decoherence. We approximate this rate by the previously calculated standard deviation δS (see App. B 1). Third, the Raman scattering rate Γ_R leads to decoherence due to decay between the two ground states. Therefore, we set the total decoherence rate as

$$\gamma = \gamma_0 + \delta S + \langle \Gamma_R \rangle_r. \quad (\text{C5})$$

Combining these results, we determine the MCN N_c for each measurement parameters (Δ_p, N) . The results are shown in the main article text (see Fig. 4).

Appendix D: Scaling factor β

The scaling factor β is the only free parameter in our model. Using a constant $\beta \sim 0.07$ for all detunings and atom numbers works already satisfactory for detunings $\Delta_p > 7\Gamma$. However, not all measured delays are as well reproduced as shown in Fig. 2(b) for $\Delta_p = 18.4\Gamma$. As β represents a scaling factor which includes the spatio-temporal dynamics of the Stokes gain, it

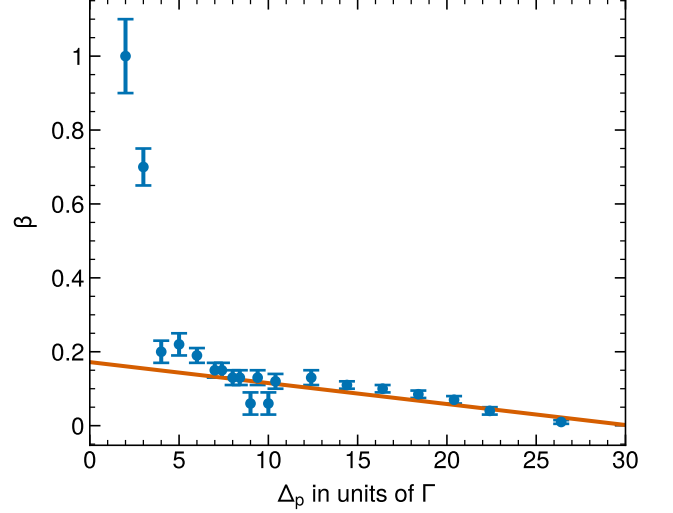


FIG. 6. Scaling factor $\beta(\Delta_p)$ as determined from manual fits to the measured $\langle t_D(N) \rangle$. The solid line shows a linear fit for $\Delta_p > 6\Gamma$ with $\beta(\Delta_p) = 0.182 - 6.1 \times 10^{-3}\Delta_p/\Gamma$.

seems reasonable to assume that β varies with the detuning (and atom number). Therefore, we plotted $\langle t_D(N) \rangle$ and determined $\beta(\Delta_p)$ by manually fitting the calculated mean delays [Eq. (2)] to the data. The resultant $\beta(\Delta_p)$ (see Fig. 6) varies approximately linearly for $\Delta_p > 6\Gamma$. The reason for such a linear dependence is currently unknown. For $\Delta_p \lesssim 6\Gamma$ β increases strongly up to 1, indicating that our model is not valid anymore in this range. This comes as no surprise as this is approximately the regime where the effective TLS model breaks down, i.e., $\Delta_p \lesssim \Omega_p$ and dispersion should become relevant. For calculating the MCN as shown in the main text we fit $\beta(\Delta_p)$ for $\Delta_p > 6\Gamma$ with a linear function yielding $\beta(\Delta_p) = 0.182 - 6.1 \times 10^{-3}\Delta_p/\Gamma$. We use this $\beta(\Delta_p)$ for all measured detunings. The origin of this linear dependence is currently unknown and will be investigated in the future trying to find a model for β .

Appendix E: Validity of the pencil-shaped model for an ensemble coupled to a HCPBGF

The pencil-shaped model can be applied when the field propagates along a single direction and transverse field variations can be neglected [4]. In free space, this is the case when the Fresnel number $F = \pi\sigma_a^2/(\lambda L) \sim 1$. In our case, the Fresnel number is $F \sim 10^{-4} \ll 1$ so a 3D description would be appropriate. However, the waveguide collects radiation emitted into a cone of opening angle $\text{NA} = \lambda/(\pi\sigma_p)$. Thus, our effective Fresnel number is $F' \sim \sigma_a/\sigma_p \sim 1$ and the pencil-shaped model can be applied.

[1] S. Haroche and D. Kleppner, *Physics Today* **42**, 24 (1989).

[2] R. H. Dicke, *Physical Review* **93**, 99 (1954).

[3] B. Bellomo, G. L. Giorgi, G. M. Palma, and R. Zambrini, *Physical Review A* **95**, 043807 (2017).

[4] M. Gross and S. Haroche, *Physics Reports* **93**, 301 (1982).

[5] W. Guerin, M. Rouabah, and R. Kaiser, *Journal of Modern Optics* **64**, 895 (2017), arxiv:1605.02439.

[6] R. Bonifacio and L. A. Lugiato, *Physical Review A* **11**, 1507 (1975).

[7] N. Skribanowitz, I. P. Herman, J. C. MacGillivray, and M. S. Feld, *Physical Review Letters* **30**, 309 (1973).

[8] R. A. de Oliveira, M. S. Mendes, W. S. Martins, P. L. Salданha, J. W. R. Tabosa, and D. Felinto, *Physical Review A* **90**, 023848 (2014).

[9] S. L. Bromley, B. Zhu, M. Bishof, X. Zhang, T. Bothwell, J. Schachenmayer, T. L. Nicholson, R. Kaiser, S. F. Yelin, M. D. Lukin, A. M. Rey, and J. Ye, *Nature Communications* **7**, 11039 (2016), arxiv:1601.05322.

[10] S. J. Roof, K. J. Kemp, M. Havey, and I. M. Sokolov, *Physical Review Letters* **117**, 073003 (2016), arxiv:1603.07268.

[11] M. O. Araújo, I. Krešić, R. Kaiser, and W. Guerin, *Physical Review Letters* **117**, 073002 (2016), arxiv:1603.07204.

[12] A. Goban, C.-L. Hung, J. D. Hood, S.-P. Yu, J. A. Muniz, O. Painter, and H. J. Kimble, *Physical Review Letters* **115**, 063601 (2015).

[13] P. Solano, P. Barberis-Blostein, F. K. Fatemi, L. A. Orozco, and S. L. Rolston, *Nature Communications* **8**, 1857 (2017).

[14] S. Okaba, D. Yu, L. Vincetti, F. Benabid, and H. Katori, *Communications Physics* **2**, 136 (2019).

[15] R. Pennetta, M. Blaha, A. Johnson, D. Lechner, P. Schneeweiss, J. Volz, and A. Rauschenbeutel, *Physical Review Letters* **128**, 073601 (2022).

[16] M. Scheibner, T. Schmidt, L. Worschel, A. Forchel, G. Bacher, T. Passow, and D. Hommel, *Nature Physics* **3**, 106 (2007).

[17] J. A. Mlynek, A. A. Abdumalikov, C. Eichler, and A. Wallraff, *Nature Communications* **5**, 5186 (2014).

[18] R. Monshouwer, M. Abrahamsson, F. Van Mourik, and R. Van Grondelle, *The Journal of Physical Chemistry B* **101**, 7241 (1997).

[19] A. Asenjo-Garcia, M. Moreno-Cardoner, A. Albrecht, H. J. Kimble, and D. E. Chang, *Physical Review X* **7**, 031024 (2017), arxiv:1703.03382.

[20] A. S. Sheremet, M. I. Petrov, I. V. Iorsh, A. V. Poshakin-skiy, and A. N. Poddubny, *Reviews of Modern Physics* **95**, 015002 (2023).

[21] M. Houde, A. Mathews, and F. Rajabi, *Monthly Notices of the Royal Astronomical Society* **475**, 514 (2018).

[22] D. Meiser, J. Ye, D. R. Carlson, and M. J. Holland, *Physical Review Letters* **102**, 163601 (2009), arxiv:0901.3105.

[23] M. A. Norcia, M. N. Winchester, J. R. K. Cline, and J. K. Thompson, *Science Advances* **2**, e1601231 (2016).

[24] J. Flick, N. Rivera, and P. Narang, *Nanophotonics* **7**, 1479 (2018).

[25] H. Tanji-Suzuki, I. D. Leroux, M. H. Schleier-Smith, M. Cetina, A. T. Grier, J. Simon, and V. Vuletić, in *Advances In Atomic, Molecular, and Optical Physics*, Vol. 60 (Elsevier Science, 2011) pp. 201–237.

[26] G. Ferioli, A. Glicenstein, F. Robicheaux, R. T. Sutherland, A. Browaeys, and I. Ferrier-Barbut, *Physical Review Letters* **127**, 243602 (2021).

[27] M. O. Scully, E. S. Fry, C. H. R. Ooi, and K. Wódkiewicz, *Physical Review Letters* **96**, 010501 (2006).

[28] J. Javanainen, J. Ruostekoski, Y. Li, and S.-M. Yoo, *Physical Review Letters* **112**, 113603 (2014).

[29] A. Ishikawa, K. Miyajima, M. Ashida, T. Itoh, and H. Ishihara, *Journal of the Physical Society of Japan* **85**, 034703 (2016).

[30] P. Andrejić and A. Pálffy, *Physical Review A* **104**, 033702 (2021).

[31] T. Bienaimé, S. Bux, E. Lucioni, Ph. W. Courteille, N. Piovella, and R. Kaiser, *Physical Review Letters* **104**, 183602 (2010).

[32] R. Bachelard, N. Piovella, and Ph. W. Courteille, *Physical Review A* **84**, 013821 (2011).

[33] T. Bienaimé, R. Bachelard, N. Piovella, and R. Kaiser, *Fortschritte der Physik* **61**, 377 (2013).

[34] E. Paradis, B. Barrett, A. Kumarakrishnan, R. Zhang, and G. Raithel, *Physical Review A* **77**, 043419 (2008).

[35] P. Weiss, A. Cipris, R. Kaiser, I. M. Sokolov, and W. Guerin, *Physical Review A* **103**, 023702 (2021).

[36] A. Kumarakrishnan and X. L. Han, *Physical Review A* **58**, 4153 (1998).

[37] G. O. Ariunbold, M. M. Kash, V. A. Sautenkov, H. Li, Y. V. Rostovtsev, G. R. Welch, and M. O. Scully, *Physical Review A* **82**, 043421 (2010).

[38] A. Angerer, K. Streltsov, T. Astner, S. Putz, H. Sumiya, S. Onoda, J. Isoya, W. J. Munro, K. Nemoto, J. Schmiedmayer, and J. Majer, *Nature Physics* **14**, 1168 (2018).

[39] F. T. Arecchi and E. Courtens, *Physical Review A* **2**, 1730 (1970).

[40] W. Guerin, M. O. Araújo, and R. Kaiser, *Physical Review Letters* **116**, 083601 (2016).

[41] K. P. Nayak, M. Sadgrove, R. Yalla, F. L. Kien, and K. Hakuta, *Journal of Optics* **20**, 073001 (2018).

[42] B. Debord, F. Amrani, L. Vincetti, F. Gérôme, and F. Benabid, *Fibers* **7**, 16 (2019).

[43] C. Liedl, F. Tebbenjohanns, C. Bach, S. Pucher, A. Rauschenbeutel, and P. Schneeweiss, *Observation of superradiant bursts in waveguide QED* (2022), arxiv:2211.08940 [physics, physics:quant-ph].

[44] S. Asselie, A. Cipris, and W. Guerin, *Physical Review A* **106**, 063712 (2022).

[45] F. Blatt, T. Halfmann, and T. Peters, *Optics Letters* **39**, 446 (2014), arxiv:1311.0635v2.

[46] T. Peters, L. P. Yatsenko, and T. Halfmann, *Physical Review A* **103**, 063302 (2021), arxiv:2101.04982.

[47] L. Ostermann, C. Meignant, C. Genes, and H. Ritsch, *New Journal of Physics* **21**, 10.1088/1367-2630/ab05fb (2019).

[48] M. G. Raymer and J. Mostowski, *Physical Review A* **24**, 1980 (1981).

[49] T. Wang and S. F. Yelin, *Physical Review A* **72**, 043804 (2005).

[50] D. A. Steck, *Rubidium 87 D Line Data*, available online at <http://steck.us/alkalidata> (2019).

[51] T. Peters, T.-P. Wang, A. Neumann, L. S. Simeonov, and T. Halfmann, *Optics Express* **28**, 5340 (2020).

- [52] D. J. Heinzen, J. E. Thomas, and M. S. Feld, Physical Review Letters **54**, 677 (1985).
- [53] F. Haake, H. King, G. Schröder, J. Haus, and R. Glauber, Physical Review A **20**, 2047 (1979).
- [54] M. G. Raymer and I. A. Walmsley, in *Coherence and Quantum Optics V* (Springer US, Boston, MA, 1984) pp. 63–70.
- [55] D. Polder, M. F. H. Schuurmans, and Q. H. F. Vrehen, Physical Review A **19**, 1192 (1979).
- [56] F. Haake, J. Haus, H. King, G. Schröder, and R. Glauber, Physical Review Letters **45**, 558 (1980).
- [57] R. Bachelard, N. Piovella, W. Guerin, and R. Kaiser, Physical Review A **94**, 033836 (2016).
- [58] K. J. Kemp, S. J. Roof, M. D. Havey, I. M. Sokolov, D. V. Kupriyanov, and W. Guerin, Physical Review A **101**, 033832 (2020).
- [59] W. Guerin and R. Kaiser, Physical Review A **95**, 053865 (2017).
- [60] M. G. Raymer, Z. W. Li, and I. A. Walmsley, Physical Review Letters **63**, 1586 (1989).
- [61] A. Bruns, C.-Y. Hsu, S. Stryzhenko, E. Giese, L. P. Yatsenko, I. A. Yu, T. Halfmann, and T. Peters, Quantum Science and Technology **8**, 015002 (2022).